Journal of Molecular Structure 1355 (2026) 145031

Contents lists available at ScienceDirect

Journal of Molecular Structure

journal homepage: www.elsevier.com/locate/molstr

Novel pillar[6]arene thin films for enhanced gas sensing of volatile organic compounds

Inci Capan [a,1], Ahmed Nuri Kursunlu [b,1], Yaser Acikbas [c], Elif Yemisci [b], Rifat Capan [a], Mustafa Ozmen [b,*]

[a] Balikesir University, Science Faculty, Physics Department, 10145, Balikesir, , Türkiye
[b] Selçuk University, Science Faculty, Chemistry Department, 42250, Konya, Türkiye
[c] Uşak University, Engineering Faculty, Electrical and Electronics Engineering Department, 64200, Usak, Türkiye

ARTICLE INFO

Keywords:
Pillar[6]arene
Spun thin film
Surface plasmon resonance
Vapor sensor

ABSTRACT

On the surface of glass substrates, pillar[6]arene based compounds (**I-P[6]**, **R1-P[6]**, **R2-P[6]**), newly synthesized, were coated using the spin coating method, respectively. AFM, SEM-EDX, and contact angle measurements were applied to characterize the films. The thicknesses of the spun P[6]-based thin films were estimated using WINSPALL software. Based on experimental and fitting data, the thickness of the spun thin film was calculated to be 1.11 nm for **I-P[6]**, 10.05 nm for **R1-P[6]**, and 10.22 nm for **R2-P[6]**. These P[6]-based compounds were then used as a new gas sensing platform for the determination of various volatile organic compounds (VOCs). Due to the better interaction, the **R1-P[6]** coated film shows a higher sensitivity and better selectivity toward VOCs than that of **I-P[6]** and **R2-P[6]** films. Therefore, important sensor parameters such as response, sensitivity, limit of detection (LOD), limit of quantitation (LOQ), response time, and recovery time for the **R1-P[6]** thin-film sensor have been elucidated. The **R1-P[6]** thin film sensor performed better against dichloromethane than the other vapors tested with a sensitivity of 26.14×10^{-4} Hz/ppm, LOD and LOQ values of 1.26 ppm and 3.82 ppm respectively. This study presents a promising gas sensing platform for rapid and sensitive analysis of some industrial aliphatic hydrocarbons.

1. Introduction

In recent years, the detection and capture of volatile organic compounds (VOCs) have gained significant attention due to their widespread impact on environmental and human health. VOCs are emitted from a numerous sources, including industrial processes, household products, and combustion engines, contributing to air pollution and posing health risks [1]. Developing effective materials for capturing and sensing VOCs is crucial for mitigating these harmful effects. There are many excellent materials used for VOC sensor applications, like calix[n]resorcinarene [2,3], cyclodextrin [4], crown ether [5], and a new generation of macrocyclic molecules in supramolecular chemistry called pillar[n]arenes (PAs) discovered by Ogoshi [6–8]. PAs have emerged as prominent receptors due to the high reactivity of the hydroquinone units that constitute the macrocyclic core of these molecules [9]. A key feature of pillar[n]arenes is their functional versatility, allowing significant modification of their physical properties by introducing functional groups at both ends of the structure. Their rigid, symmetrical design and tunable properties facilitate easy functionalization. With their electron-rich cavities, pillar[n]arenes have garnered interest for applications such as artificial ion gates [10], drug delivery [11,12], and sensors [13,14]. Since 2008, they have been explored for vapor sensor applications due to their variable cavity dimensions and ability to be tailored for specific vapor molecules through various non-covalent interactions like π – π stacking, cation - π, CH - π interaction, and hydrogen bonding. There exists a substantial gap in the literature between the synthesis of new pillar[n]arene materials and the investigation of their vapor sensing properties. For example, Feng and et al. utilized pillar [5] arene compounds to detect n-alkane vapors (hexane, pentane, heptane), which are suitable for host-guest interactions [15]. Decaalkyne pillar [5] arene and bibenzyl chloride were constructed for the adsorption of iodine vapor because the pillar[5]arene macrocycle has several adsorption sites, including aromatic rings, diynes, and oxygen atoms. Their results indicated that linking electron-rich pillar[5]arene

* Corresponding author.
E-mail address: musozmen@gmail.com (M. Ozmen).
[1] These authors contributed equally to this work.

https://doi.org/10.1016/j.molstruc.2025.145031
Received 12 August 2025; Received in revised form 27 October 2025; Accepted 7 December 2025
Available online 8 December 2025

macrocycles exhibited highly effective iodine capture with a reasonable recyclability [16]. A fluorescence turn-on sensing pillar[4]arene against ethylenediamine (EDA) vapor was used to study the physical adsorption of EDA. The results showed that pillar[4]arene is suitable for facile fluorescence turn-on sensing of EDA vapor to distinguish EDA from other aliphatic amines [17].

Pillar[n]arenes can form stable host-guest complexes with various organic molecules [18,19], particularly due to the moderate cavity size of pillar[5]arene, which is advantageous for interacting with small, volatile molecules. By modifying the structure, researchers can optimize selectivity and responsiveness to specific VOCs [20]. Pillar[6]arene, with its larger cavity size, accommodates a diverse range of guest molecules, enhancing its applicability [21]. The cavity size of approximately 6.7 Å allows pillar[5]arenes to engage with hydrocarbons, aromatic systems, and cationic species through hydrophobic forces, Van der Waals interactions, and other binding mechanisms [22]. By modifying the functional groups on pillar [6]arene rings, researchers can fine-tune their affinity, selectivity, and stability for specific VOCs [23], making them highly adaptable to different sensing and adsorption requirements [24,25].

Our recent studies are concentrated on the vapor sensor abilities of pillar[5]arene thin films prepared by Langmuir-Blodgett (LB) [1,26–30] and spin coating thin film techniques [20,31] using Quartz Crystal Microbalance (QCM) and Surface Plasmon Resonance (SPR) measurement techniques. A wide range of VOCs, containing aromatic to aliphatic hydrocarbons, was investigated by our group. Using the spin coating film preparation method, aromatic BTX (benzene, toluene, xylene) hydrocarbons of the pillar [5]arene thin film, including pyridine units, were investigated, and benzene vapor indicated the best performance with a high diffusion coefficient [31]. Another detailed investigation was carried out for the pillar[5]-arene, including iodines or azides and 4-hydroxybenzaldehyde or N,N-dimethyl ethylenediamine spun thin films versus dichloromethane, chloroform, carbon tetrachloride, ethyl acetate, trichloroethylene, and formic acid [20]. The best performance was yielded for dichloromethane vapor. As a result of these studies can be concluded that pillar [5]arene materials are suitable for the detection of chlorine based vapor than for investigating other vapors. Overall, the literature listed above for pillar [5]arene compound against dichloromethane vapor yielded a sensitivity of up to 7.61 Hz/ppm [27]. In this study, we have chosen pillar[6]arene compounds to improve the vapor sensor properties.

In the existing literature, the majority of studies have concentrated on the applications of pillar[5]arene derivatives while the potential of pillar[6]arene remains underexplored, enabling a comparison of the advantages of using these 5- and 6-unit compounds. Combined with its larger cavity and greater structural flexibility, pillar[6]arene presents new possibilities for developing advanced gas sensors. This study is focused on the synthesize of novel pillar[6]arene derivatives and their use in VOC sensor applications. To our knowledge, this represents the first investigation of its kind documented in the literature. The molecular structures of pillar[6]arene were designed appropriately as to the diameter of organic solvents for a better interaction. A reagent and two final products (**I-P [6]**, **R1-P [6]**, and **R2-P [6]**) are tested as a sensing materials for the recognition of volatile pollutants in industrial regions. Among these P[6]-based compounds, the **R1-P[6]** thin film sensor performed a better sensor performance in terms of sensitivity, limit of detection (LOD), and limit of quantification (LOQ) values. The sensor parameters for the pillar[6]arene fabricated *via* the spin coating technique are compared to the sensor parameters calculated for pillar[5]arene in our previous studies. The obtained results for pillar [6]arene compound against dichloromethane vapor showed that the sensitivity value can increase approximately four times higher than pillar[5]arene compounds.

2. Experimental details

2.1. Materials and instruments

All chemicals were obtained from commercial suppliers (Sigma-Aldrich, Thermo Scientific, Isolab Chemicals, and Acros) and used without any additional purification. NMR spectra were recorded on a Bruker AV-400 spectrometer operating at 400 MHz. FT-IR spectra (4000–400 cm^{-1}) were collected at each stage using a PerkinElmer 100 spectrophotometer. Elemental analysis was performed with a Truspec elemental analyzer. The synthesis reagents; 4-(prop-2-yn-1-yloxy) benzaldehyde, 1,4-bis(2-bromoethoxy)benzene, and 1,4-bis(2-iodoethoxy)benzene were prepared and characterized according to previously reported procedures [20,32,33]. The synthesis details are given in Supplementary Information. Then, Br-P[6], N_3-P[6] and **I-P [6]** were firstly prepared for the final products, **R1-P [6]** and **R2-P [6]** (Scheme 1). The morphology, homogeneity, and hydrophilic/hydrophobic character of the pillar[6]arene based films were investigated *via* Atomic Force Microscopy (AFM, NT-MDT AFM NTEGRA Solaris), Scanning Electron Microscopy (SEM, Zeiss EVO LS10), and Contact Angle Measurements (Krüss FM40Mk2 Easy Drop).

2.2. Film preparation and gas sensor measurements

The spin coating technique is based on the overspreading of the solution in a volatile solvent released onto a rotating substrate with a predetermined value of rotation speed with a predetermined value of rotation speed *via* the centrifugal force. The spin coating thin film fabrication method facilitates the fast organization of the pillar[*n*]arene molecules on the surface of a substrate. This method is preferable for producing thin films because it uses a minimum amount of deposition material and enables rapid production. Furthermore, the ability to control film thickness, the simplicity of the process, low production cost, and the fact that annealing is not required make it possible to prepare homogeneous thin films using this technique, which is necessary for chemical sensor applications. 50 nm thick gold layer coated glass substrates were supplied from TEKNOTIP/TURKEY with dimensions of 20 mm × 20 mm as the substrate for the fabrication of the spun thin films. A SCS G3P-8 spin coating device was employed for the fabrication of the spun thin films. 100 μL of pillar[*n*]arene solution with the concentrations of 3.5 mg mL^{-1} for **I-P [6]** and 2.0 mg mL^{-1} for **R1-P [6]** and **R2-P [6]** molecules was released onto the substrate shortly before its movement using a microliter syringe. During the formation of the layer, 3 steps of fabrication routine was used; the substrate was brought to a rotation speed of 500 rpm in 10 s, and then increased to 1000 rpm in another 10 s keeping the rotation speed constant for 25 s, and in the last step deceleration through the standing still position lasted for 10 s which generates the total thin film formation time of 55 s. At least 30 min were allowed for the thin film to evaporate any residual solvent, which may collapse in the bulk volume of the thin film.

The gas sensing characterization was performed with the SPR setup, Biosuplar 6 model SPR system with a He-Ne laser (632.8 nm) and an angular resolution of 0.003°. A glass prism was mounted onto a holder to provide the Kretschmann configuration to generate the surface plasmons. The p-polarized beam is totally internal reflected when directed above the critical angle. At a special angle θ_{SPR} the SPR formation is supplied between the interface gold/thin film (metal/dielectric) *via* their negatively signed dielectric constants, exciting the delocalized electrons of the gold layer, bringing them into resonance. Therefore, the reflected light intensity experiences a dramatic decrease at the θ_{SPR}. For the gas sensing experiments, dichloromethane, chloroform, ethyl acetate, carbon tetrachloride with a purity of 99% (Sigma-Aldrich), trichloroethylene with a purity of 99% (Thermo Scientific), and formic acid with a purity of 85% (Isolab Chemicals) were used without further purification. The saturated vapors were supplied by filling the half volume of a glass flask with the liquid form of the volatile solvents at

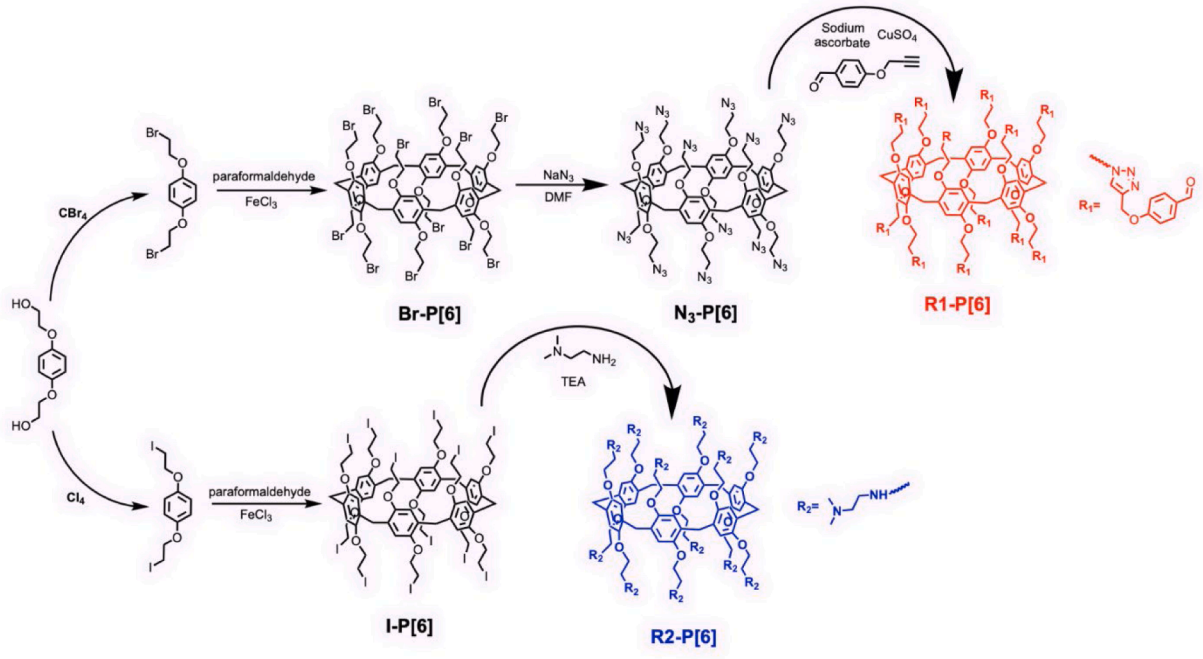

Scheme 1. Synthesis route of **I-P [6]** , **R1-P [6]** , and **R2-P [6]** compounds.

room temperature; therefore, the saturated vapor will fulfill the other half. The saturated form of each VOC was transferred into a 1 mL injector to expose it to the gas cell. The gas sensing measurements were performed in 4 steps; 0.25 mL of saturated vapor was mixed with dry air to reach a volume of 1 mL, where in each step the saturated vapor volume was increased by 0.5 mL, 0.75 mL, and the rest of the volume was completed with dry air. In the last step, 1 mL of the volume was fulfilled with saturated vapor only. The exposures of the vapor and flushing with the dry air lasted for 2 min each, periodically. The reciprocal exposures of the saturated vapor were used to monitor the

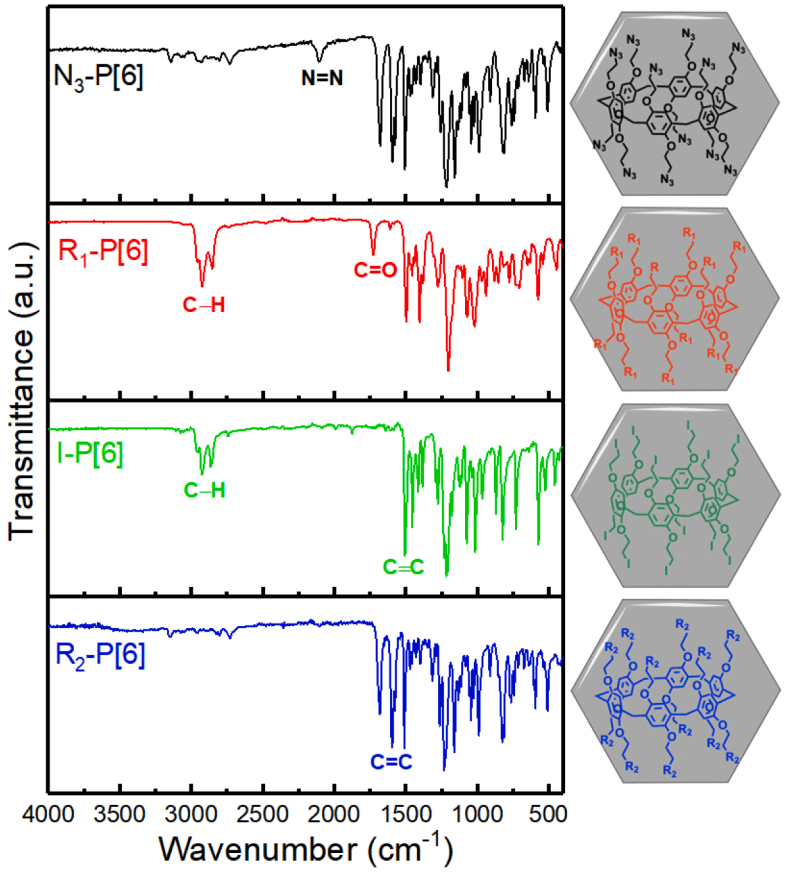

Fig. 1. FTIR spectra of N_3-P[6], **R1-P [6]** , **I-P [6]** , and **R2-P [6]** compounds.

reproducibility of the pillararene thin film sensors. All measurements were performed at room temperature (25 °C), and the relative humidity (RH) value was 25% which is monitored by HTC-2 LCD Digital Thermometer Hygrometer.

3. Results and discussion

3.1. Characterization of compounds and morphological analysis of the P[6]-based spun films

As described in the synthesis details, **R1-P[6]** was obtained with a click reaction mechanism from N_3-P [6] compound, while **R2-P[6]** was prepared with **I-P[6]** macro ring. The synthesis of compounds was characterized with FT-IR spectroscopy and illuminated to the functional groups of the target compounds (Fig. 1).

First of all, N_3-P [6] shows a clear curve that the most characteristic band assigned $N = N$ vibrations in the azide moieties was observed around 2070 cm^{-1}. The other peaks of N_3-P[6] such as $C = C$, C—H, C—O etc. raised at the expected regions. After the triazole transformation of N_3-P[6] to **R1-P[6]** with click reaction, the classical azide vibration disappeared while the other peaks shifted to down-field or up-field. Moreover, the small fragments of **R1-P[6]** (aldehyde terminals), $C = O$ stretching vibrations were newly observed around 1700 cm^{-1}. On the other hand, the FT-IR spectra of **R2-P[6]** and its reagent material, **I-P[6]**, are significantly different from each other. So, the several peaks between the 1600 and 1700 cm^{-1} are also available in the spectrum of **R2-P[6]**, while the spectrum of **I-P[6]** has classical $C = C$ bonding vibrations assigned aromatic units and C—O stretching vibrations. All spectral changes show to the successful synthesis of the reagent and target compounds.

The ^{1}H NMR and ^{13}C NMR spectra of pillar[6]arene derivatives were also performed (Fig. S1-S8). The bridge CH_2-protons of these compounds are observed around 3.8–4 ppm as multiplet form, while the aromatic hydrogens on the main skeleton appear as singlet between 6.7–7 ppm. After the synthesis of **R1-P[6]**, the triazole-protons and other phen-protons gave several signals such as doublet or singlet while the aldehyde protons of **R1-P[6]** was observed at 9.8 ppm in ^{1}H NMR spectrum. The ^{1}H NMR spectrum of **R2-P[6]** presented a lot of peaks around 2 and 4 ppm belonging to different alkyl groups (chain-CH_2's and CH_3's) while NH-protons appeared around 4.5 ppm. Moreover, the protons of two linkage-CH_2 moieties was seen around 5 ppm in ^{1}H NMR spectrum of **R1-P[6]**.

Fig. 2 presents two-dimensional (2D) and three-dimensional (3D) atomic force microscopy (AFM) images of the bare glass surface and the films coated with pillar[6]arene, and its derivatives, illustrating the homogeneous and smooth morphology of the resulting films. The surface roughness parameters, measured over a 5 × 5 μm area, revealed root-mean-square (rms) roughness values of 0.32 nm and 0.42 nm for the bare glass substrate, 0.68 nm and 0.93 nm for the **I-P[6]** film, 2.20 nm and 4.49 nm for the **R1-P[6]** film, and 1.46 nm and 2.39 nm for the **R2-P[6]** film, respectively. Surface wettability was evaluated through water contact angle measurements, yielding values of 8.71±1.13° for bare glass, 48.72±0.96° for the **I-P[6]** coated surface, 28.45±1.33° for the **R1-P[6]** coated surface, and 52.22±1.09° for the **R2-P[6]** coated surface (inset of Fig. 2). These results indicate that the hydrophobicity of the coated surfaces increased relative to the bare glass substrate. However, the presence of hydrophilic groups within the molecular structures of the coatings limited the overall increase in surface contact angles. Additionally, scanning electron microscopy (SEM) images revealed distinct morphological differences among the **I-P[6]**, **R1-P[6]**, and **R2-P[6]** coated surfaces. Elemental analysis *via* energy-dispersive X-ray spectroscopy (EDX) further characterized the elemental composition of these coatings (Fig. S9-S10).

3.2. Optical parameters of pillar[6]arene thin films

The reflected light intensity was monitored with the angle of incidence to record the SPR curves of the metal and/or thin film layers. The reflected light intensity experiences a dramatic decrease in the case of the SPR at the critical angle θ_{SPR} where the maximum energy is absorbed, this angle is dependent on the optical constants of the prism and the metal film [34] ε_P and ε_M represents the dielectric constants of the prism and the metal layer.

$$\theta_{SPR} = \sin^{-1}\left(\frac{\varepsilon_M}{\varepsilon_P(\varepsilon_M + 1)}\right)^{1/2} \quad (1)$$

In the case of a thin film formation on the metal layer, the SPR is shifted according to Eq. (1), where d is the thickness of the added layer, λ is the wavelength of the light beam, and ε is the dielectric constant of the thin film.

$$\Delta\theta_{SPR} = \frac{(2\pi/\lambda)(|\varepsilon_M|)^{3/2}d}{\sqrt{\varepsilon_P}\cos\theta(|\varepsilon_M - 1|)^2\varepsilon}(\varepsilon - 1) \quad (2)$$

Using a special software, the thickness and/or the optical constants of the thin film can be estimated. WINSPALL software was used to evaluate the SPR curves presented in Fig. 3 to estimate the thickness of the thin films, which was written by Wolfgang Knoll, developed at the

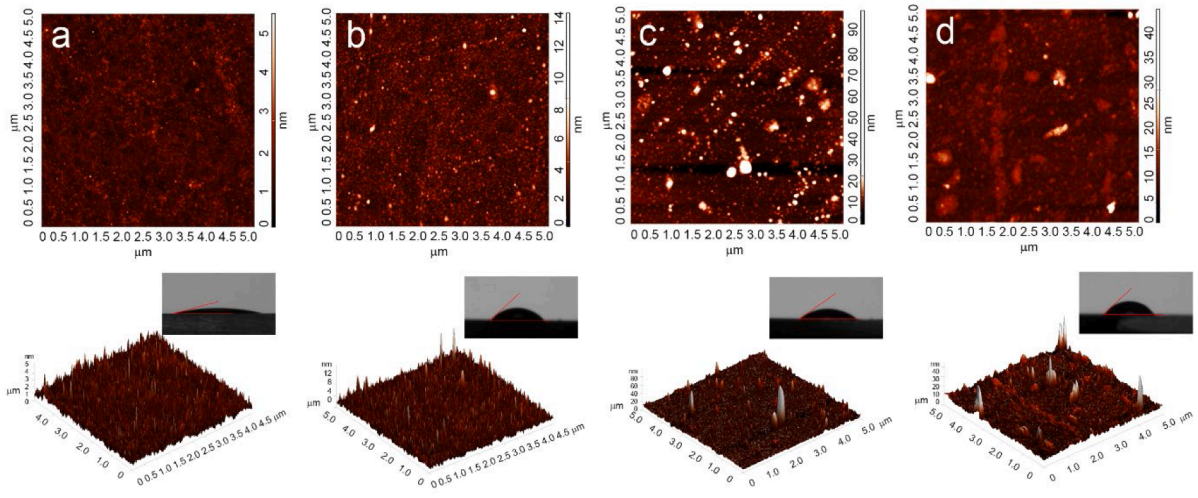

Fig. 2. 2D and 3D AFM images of bare glass (a), **I-P[6]** (b), **R1-P[6]** (c), and **R2-P[6]** (d) coated glass substrates. inset: water contact angle measurements of bare and coated films.

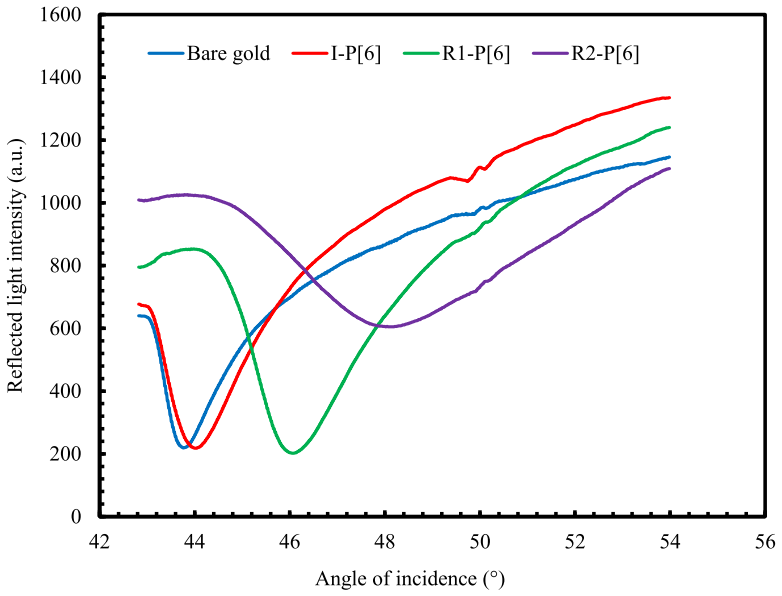

Fig. 3. SPR curves of bare gold and P[6]-based thin films.

Max-Planck Institute for Polymer Research, Germany [34]. The refractive index of the **I-P [6]** thin layers was acknowledged as 1.5, referring to the literature [35].

The thickness of the spin coated **I-P [6]** thin film was estimated as 1.11 nm, **R1-P [6]** as 10.05 nm, and **R2-P [6]** as 10.22 nm. In Fig. S11-S14, the WINSPALL fitting is presented, including both experimental and accompanying fitted data. Referring to the SPR curves presented in Fig. S11-S14, it is not a surprise to have a thin film with a thickness of just 1 nm when the SPR curve of the pillar is compared with the SPR curve of bare gold. The shift of the SPR angle minima was having its minimum value compared with the SPR curves of **R1-P [6]** and **R2-P [6]**. The shift of the SPR curve was very little, implying a quite thin layer. The SPR curve of the **R1-P [6]** compared with the gold layer shows the formation of a thin film on the gold surface having a similar amount of reflected light intensity value with the gold layer at its SPR minimum angle. The **R2-P [6]** also shows a right shift with respect to the uncoated gold substrate; however, the SPR curve was broader, which means an increase in the reflectance minimum. The critical angle was less obvious in the SPR curve of the **R2-P [6]** thin film. All this process is affected by the formation nature of the thin layers on the surface of the gold layer which depend on the chemical composition of the coating molecule and its binding features.

R1-P [6] compound has multi triazole fragments that it composes an electronic framework in the molecular hole of pillar [6]arene. It provides an excellent interaction with the test solvents in their detection. On the other hand, the amino-alkyl chains of **R2-P [6]** enable a larger cavity due to the rotation of single bonds around themselves. Thus, more branched molecules can be caught by **R2-P [6]** with intermolecular interactions. The detection mechanisms are different for **R1-P [6]** and **R2-P [6]** owing to their structural properties. However, both macrorings have a lot of hydrogen bonds and dipole-dipole interactions.

An extensive study working on SPR resonance shifts for different thin films with different dielectrics was published, analyzing the evanescent field at the metal/dielectric interface [36]. The SPR curve of the **I-P [6]** thin film with *An sprc*urve very similar to uncoated gold layer, suggesting the quite thin layer which the vapor molecules will likely have difficulty in responding and diffusing into the structure of the thin layer. Therefore, the **I-P [6]** thin film layer was not studied extensively as a gas sensing device. As to the **R2-P [6]** thin film, the broad SPR curve, additionally accompanied by a high value of the reflected light intensity during the SPR angle, was not found suitable to explore through the exposure of the vapor molecules. Both thin films exposed to several VOCs and SPR kinetic measurements are given in Figs. 4–5.

It is clear that no reasonable results were yielded during the interaction between VOC molecules and **I-P [6]** or **R2-P [6]** thin films. In addition, these responses for both thin films are not notable and stable. Therefore, no further sensor analysis for these two thin films has been made in this study.

3.3. Sensor parameters of R1-P[6] thin film

The SPR kinetic measurements were presented in Fig. 7. The response is presented in terms of the

$$Response = \frac{\Delta I}{I_o} x100 \tag{3}$$

where ΔI describes the difference in the reflected light intensity before the interaction between the thin film and vapor molecules (I_0) and after exposure to selected vapor molecules (I).

Generally, the sensing mechanism (given in Fig. 6) can be performed in five steps (initial baseline, adsorption, diffusion, desorption and reestablishment of the baseline). In this work, dichloromethane, chloroform, ethyl acetate, trichloroethylene, formic acid, and carbon tetrachloride vapors were selected as harmful organic vapors for the SPR kinetic studies. In the early baseline, the P[6]-based thin film sensor was exposed to dry air for 120 s, during which the response remained stable. The initial response of the **P [6]**-based thin film sensor showed a sharp increase for all harmful organic vapors between 120, and 125 s due to the surface adsorption effect. Once the vapor molecules have been transported into the **P [6]**-based thin film, the bulk diffusion effect takes over and the response decreases exponentially. At 240 s, the response to dry air decreased instantaneously, followed by a recovery process (between 240 and 244 s) for all harmful organic vapors due to desorption of the vapors. The response of the **P [6]**-based thin film sensor is stable after 245 s, and the sensor returns to the initial baseline.

The reciprocal exposures of the vapor molecules with the dry air, with a period of 2 min, reveal the reversible response of the **R1-P [6]** thin film. In each cycle of interaction, the increasing amount of vapor molecules was exposed, and the concentration of the vapor molecules was calculated *via* Eq. (4) given below [37]:

$$c = \frac{22.4\rho V}{MV_0} x10^6 \tag{4}$$

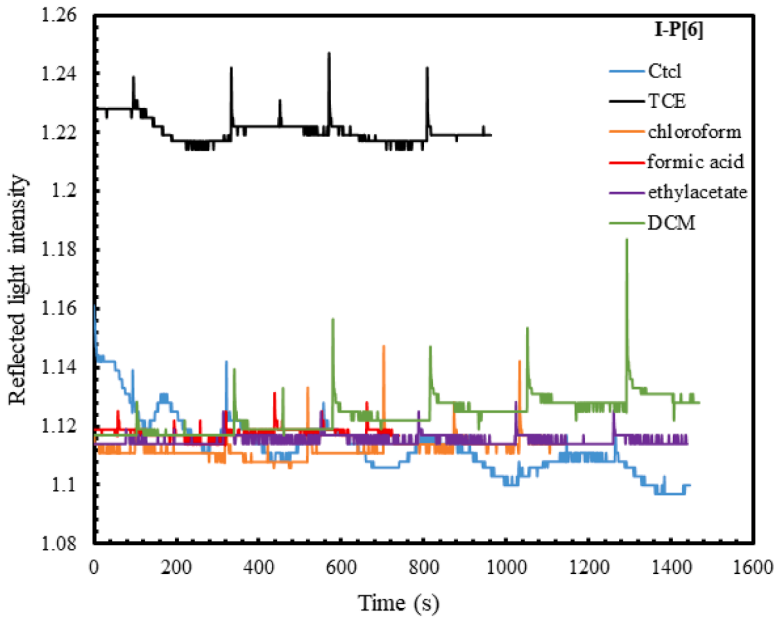

Fig. 4. SPR kinetic measurement for **I-P [6]** thin film.

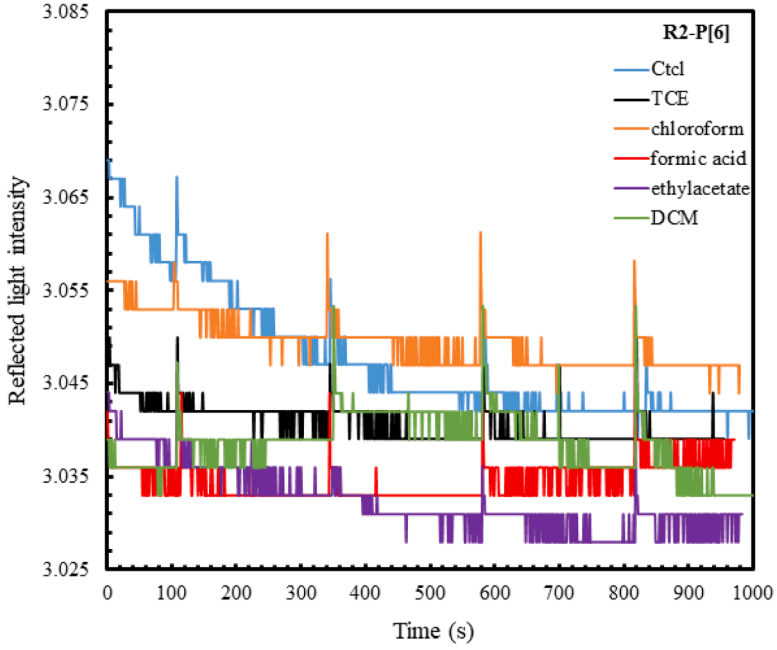

Fig. 5. SPR kinetic measurement for **R2-P [6]** thin film.

where V_0 is the volume of the gas cell, V is the volume of injected vapor into the gas cell, ρ is the density of selected vapor, and M is the vapor molecular weight. The calculated vapor concentrations were 17,500, 14,000, 11,500, 12,500, 29,700, and 11,500 ppm for dichloromethane, chloroform, ethyl acetate, trichloroethylene, formic acid, and carbon tetrachloride vapors, respectively.

To study the reproducibility and stability tests, a constant concentration value (100%) for each vapor is selected to obtain 3 cycles as a function of time, as shown in Fig. 8. The mean value and standard deviation of reproducibility cycles are calculated using Fig. 8 and given in the inset in Fig. 8.

The kinetic measurements were analyzed through the sensor parameters such as the sensitivity (S), limit of detection (LOD), limit of quantification (LOQ), response, and recovery times.

Sensitivity was calculated as:

$$S = \frac{Response}{c} \tag{5}$$

in terms of ppm^{-1} which represents the response per unit concentration of vapor molecules. Concentration dependence calibration curves of **R1-P [6]** thin film is given in Fig. S15. The calibration curves are generated for this purpose, which present the linear relation between the response and increasing concentration of each vapor. The S values are calculated using this linear relationship and are listed in Table 1. The highest S value is obtained for dichloromethane vapor, and the lowest S value for trichloroethylene vapor.

The LOD value of a sensor material describes the lowest amount of the selected vapor that can be detected. LOQ value is known as the

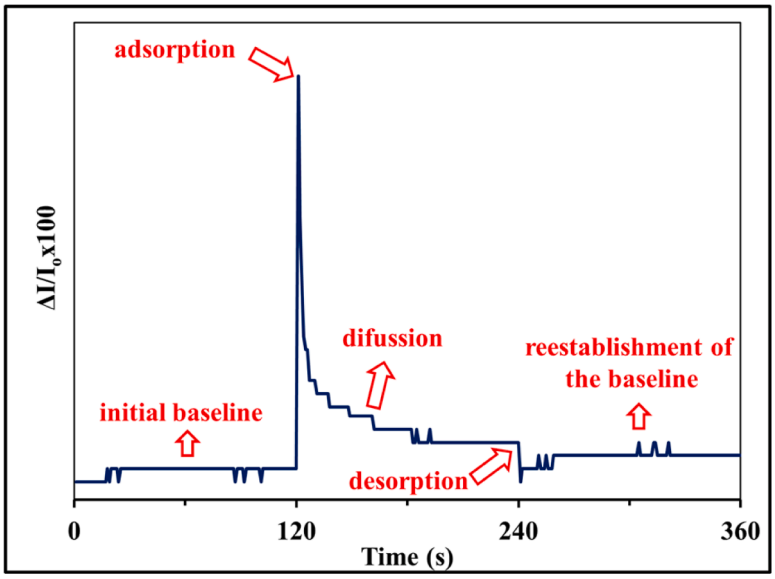

Fig. 6. A schematic diagram of the SPR sensing mechanism.

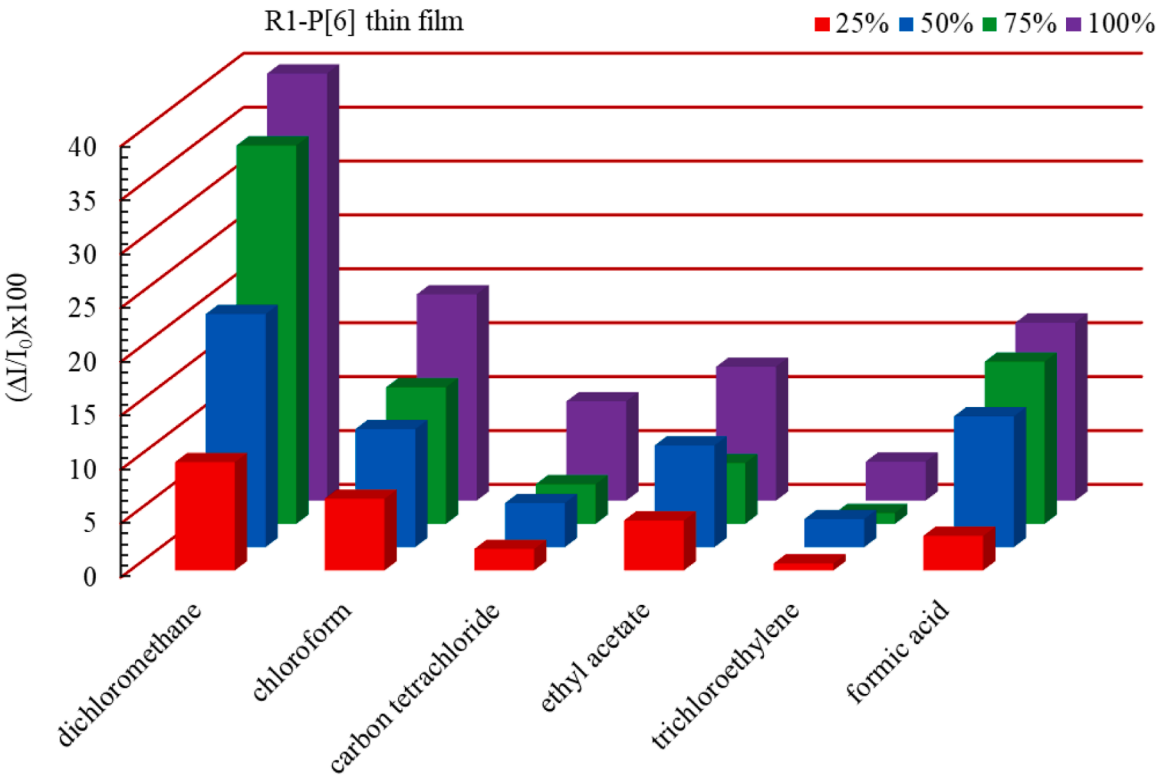

Fig. 7. The kinetic response of the **R1-P [6]** thin film.

lowest amount of the selected vapor that can be accurately quantified. These two important sensor parameters indicate a higher sensitivity and precision of a sensor material. The LOD [38] and the LOQ [39] values can be given as:

$$LOD = \frac{3.3\sigma}{S} \quad (6)$$

$$LOQ = \frac{10\ \sigma}{S} \quad (7)$$

where σ is the standard deviation for our SPR measurements (0.001) and S is the sensitivity of **R1-P [6]** thin film.

In this study, the responses of P[6]-based thin films to six different organic vapors were recorded using SPR kinetic measurements. These response data and the calculated sensor parameters are shown in Table 1.

Physical property parameters given in Table 2, such as vapor pressure, dipole moment, and molar volume of the vapors tested, can explain the measured and calculated sensor parameter values (response, sensitivity, LOD, LOQ, response and recovery times) for the **R1-P [6]** thin film sensor [40,41].

The **R1-P [6]** thin-film sensor performed with the highest response

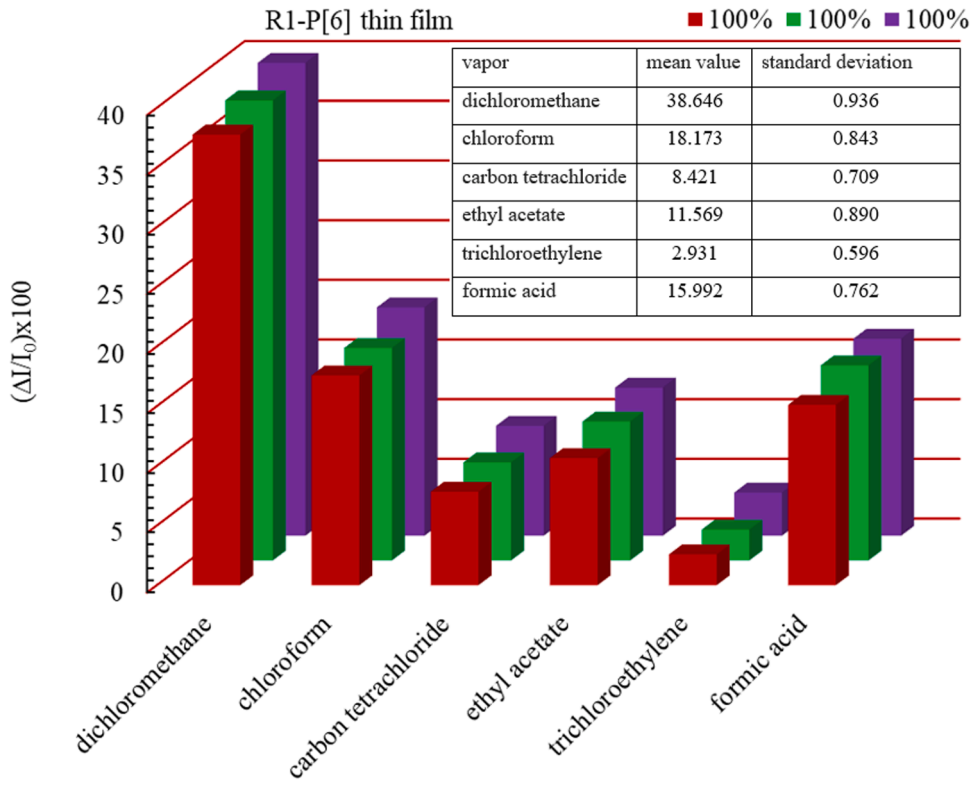

Fig. 8. The saturated vapor exposure of **R1-P [6]** thin film at the same concentration.

Table 1
The sensor parameters for **R1-P [6]** thin film compared with the previous study.

Material	VOCs	Response time (s)	Recovery time (s)	Sensitivity (response/ppm)×10^{-4}	LOD (ppm)	LOQ (ppm)	R^2	Reference
P [5]−1	Dichloromethane	-	-	4.83	6.83	20.69	0.984	[20]
	Chloroform	-	-	3.91	8.45	25.59	0.975	
	Carbon tetrachloride	-	-	2.83	11.65	35.31	0.960	
	Ethyl acetate	-	-	2.09	15.74	47.71	0.971	
	Trichloroethylene	-	-	1.91	17.25	52.27	0.983	
	Formic acid	-	-	1.42	23.16	70.17	0.999	
P [5]−2	Dichloromethane	-	-	2.25	14.68	44.48	0.982	[20]
	Chloroform	-	-	2.93	11.26	34.12	0.991	
	Carbon tetrachloride	-	-	1.60	20.65	62.58	0.968	
	Ethyl acetate	-	-	1.17	28.08	85.11	0.978	
	Trichloroethylene	-	-	1.51	21.91	66.40	0.987	
	Formic acid	-	-	0.53	62.26	188.68	0.980	
R1-P [6]	Dichloromethane	2	17	26.14	1.26	3.825	0.968	this study
	Chloroform	2	16	13.65	2.42	7.32	0.9882	
	Carbon tetrachloride	3	14	6.7	4.92	14.925	0.9435	
	Ethyl acetate	3	19	10.48	3.15	9.54	0.9125	
	Trichloroethylene	2	25	2.49	13.21	40.03	0.854	
	Formic acid	2	16	11.86	2.78	8.43	0.9411	

Table 2
Physical properties of VOCs and response values of the **R1-P [6]** thin film.

VOCs	Dipole moment (D)	Molar volume (cm^3 mol^{-1})	Vapor pressure (kPa, 25 °C)	R_1-P [6] response ($\Delta I/I_o \times 100$)
Dichloromethane	1.60	64.10	46.53	34.89
Chloroform	1.08	80.70	26.66	17.78
Carbon tetrachloride	0	97.10	15.06	5.75
Ethyl acetate	1.78	97.80	12.13	12.06
Trichloroethylene	0.80	89.70	7.73	3.40
Formic acid	1.41	37.80	4.53	30.11

($\frac{\Delta I}{I_o} x100$) and sensitivity to dichloromethane vapor. This result can be explained by the fact that dichloromethane vapor has a high vapor pressure and dipole moment compared to other vapors. It also has a low molar volume, which allows it to diffuse more quickly into the thin film sensor. Similarly, the **R1-P [6]** thin film sensor showed the highest sensitivity to dichloromethane vapor, resulting in the lowest LOD and LOQ of the thin film sensor. It was predicted that the ethyl acetate vapor molecule would be slower and more difficult to diffuse into **R1-P [6]** thin films due to its lower vapor pressure and the highest molar volume compared to the others. However, due to ethyl acetate having the highest dipole moment, the **R1-P [6]** chemical sensor exhibited relatively higher sensitivity and response to carbon tetrachloride and trichloroethylene vapors. Similarly, the thin film sensor showed a

significant response and sensitivity to formic acid vapor. This result can be interpreted as follows: The formic acid molecule has the lowest molar volume value, so it can diffuse more easily into **R1-P [6]** -based thin films, despite having the lowest vapor pressure value. These values are presented in Table 1 to compare with the sensor parameters obtained for the P [5]−1 and P [5]−2 thin-film sensors developed in our previous study [20]. From this table, it can be seen that the calculated **R1-P [6]** thin-film sensor sensitivities are higher for six different vapors than those obtained for P [5]−1 and P [5]−2 thin-film sensors. In particular, the sensitivity values of the **R1-P [6]** sensor for the vapors of dichloromethane, ethyl acetate, and formic acid show a significant increase. Comparing the sensitivities of the P[5]−1 and P[5]−2 chemical sensors with **R1-P [6]** against dichloromethane vapor, the **R1-P [6]** chemical sensor yielded approximately 5.4 and 11.6 times higher sensitivity than two sensors. A similar comparison was observed for ethyl acetate vapor, ~ 5.0 and ~ 9.8 times, and for formic acid vapor, ~ 8.3 and ~ 22.3 times, respectively.

In addition, one of the reasons for the higher efficiency of the **R1-P [6]** sensor in the detection of organic vapors is the increase in intermolecular interaction. There may be more intermolecular interactions between the multi nucleophilic groups, such as nitrogen, oxygen, and aromatic rings on the compounds that make up the **R1-P [6]** sensor material. Although the possibility of the same interactions occurring between P[5]-based molecules and vapor molecules is high, the more efficient performance of the **R1-P [6]** sensor compared to P [5]-based sensors can be explained by the molecular structures of the P [5] and **R1-P [6]** materials. Because the radius of the **R1-P [6]** molecule is larger than that of the P[5] molecules, and therefore the electronic lattice is more convenient, the intermolecular interaction will be relatively greater. As the **R1-P [6]** molecule has a more ideal cavity, it will capture vapor molecules more easily.

4. Conclusion

Here, we investigated the sensor performance of a reagent (**I-P [6])** and two novel final products (**R1-P [6]** and **R2-P [6])** as sensing materials against some industrial aliphatic hydrocarbons and examined whether they provide a promising gas sensing platform. In order to synthesize and characterize these novel compounds, ^{1}H and ^{13}C NMR and FT-IR spectral techniques were employed. The preparation of **I-P [6] , R1-P [6] ,** and **R2-P [6]** thin films, for the first time, onto the gold-coated glass substrate was successfully and uniformly achieved by using the spin coating technique. The prepared **P [6] -**based thin film surfaces were characterized by AFM, SEM-EDX, and contact angle measurements. In addition, the thicknesses of these spun films were predicted by using the experimental data of SPR curves and fitting data obtained from WINSPALL software. The SPR technique was also used to investigate gas sensing properties of **P [6] -**based thin film against six different industrial aliphatic hydrocarbons. Among these hydrocarbons tested, the **R1-P [6]** thin film sensor showed the highest response to dichloromethane vapor. This result was supported by the sensor performance parameters of the **R1-P [6]** thin-film sensor against dichloromethane such as response time (2 s), recovery time (17 s), sensitivity (26.14×10^{-4} Hz/ppm), LOD (1.26 ppm) and LOQ (3.82 ppm).

The performance of the **R1-P [6]** thin film sensor was also compared with the sensor parameters obtained for the **P [5] −1** and **P [5] −2** thin film sensors developed in our previous study. The **R1-P [6]** chemical sensor was found to be about 5.41 and 11.61 times more sensitive to dichloromethane than the **P [5] −1** and **P [5] −2** chemical sensors, respectively. A similar comparison was observed for the formic acid vapor, ~ 8.35 and ~ 22.37 times, and for the ethyl acetate vapor, ~ 5.01 and ~ 9.85 times, respectively. These results and comparisons can be explained by the superiorities of **P [6]** -based compounds compared to **P [5]** -based compounds, such as larger radius, more convenient electronic lattice, larger intermolecular interactions, and more ideal cavities.

CRediT authorship contribution statement

Inci Capan: Writing – original draft, Validation, Methodology, Investigation, Formal analysis, Data curation, Conceptualization. **Ahmed Nuri Kursunlu:** Writing – original draft, Investigation, Funding acquisition, Data curation, Conceptualization. **Yaser Acikbas:** Writing – original draft, Validation, Methodology, Investigation, Formal analysis. **Elif Yemisci:** Validation, Methodology, Investigation, Formal analysis. **Rifat Capan:** Writing – review & editing, Writing – original draft, Validation, Methodology, Data curation, Conceptualization. **Mustafa Ozmen:** Writing – review & editing, Writing – original draft, Methodology, Investigation, Formal analysis, Data curation, Conceptualization.

Declaration of competing interest

The authors declare that they have no known competing financial interests or personal relationships that could have appeared to influence the work reported in this paper.

Acknowledgments

We would like to thank Selcuk University (BAP Project Number: 22408005) for funding this study.

Supplementary materials

Supplementary material associated with this article can be found, in the online version, at doi:10.1016/j.molstruc.2025.145031.

Data availability

No data was used for the research described in the article.

References

[1] A.N. Kursunlu, Y. Acikbas, M. Ozmen, M. Erdogan, R. Capan, Preparation of pillar [5]arene-quinoline Langmuir–Blodgett thin films for detection of volatile organic compounds with host–guest principles, Analyst 142 (2017) 3689–3698.
[2] P. Clément, E. Llobet, Chapter seven - carbon nanomaterials functionalized with macrocyclic compounds for sensing vapors of aromatic VOCs, in: R. Jaaniso, O.K. Tan (Eds.), Semiconductor Gas Sensors (Second Edition), Woodhead Publishing2020, pp. 223–37.
[3] S. Şen, F. Davis, R. Çapan, Z. Özbek, M.E. Özel, G.A. Stanciu, A macrocyclic tetraundecyl calix [4]resorcinarene thin film receptor for chemical vapour sensor applications, J. Incl. Phenom. Macrocycl. Chem. 98 (2020) 237–247.
[4] B. Phillips, H.L. Abani, P. Wei, C. Li, M. Zhao, J. Handy, S. Banerjee, H.J. Sue, E. Pentzer, M. Al-Hashimi, H.C. Zhou, L. Fang, Inverse emulsion-crosslinked cyclodextrin polymer nanoparticles for selective adsorption and chemiresistive sensing of BTEX, Mater. Today Chem. 24 (2022) 100915.
[5] J.-S. Shih, Piezoelectric crystal membrane chemical sensors based on fullerene and macrocyclic polyethers, J. Chin. Chem. Soc. 47 (2000) 21–32.
[6] L.E. Khalil-Cruz, P. Liu, F. Huang, N.M. Khashab, Multifunctional pillar[n]arene-based smart nanomaterials, ACS Appl. Mater. Interfaces. 13 (2021) 31337–31354.
[7] T. Ogoshi, S. Kanai, S. Fujinami, T.A. Yamagishi, Y. Nakamoto, *Para*-bridged symmetrical pillar [5]arenes: their lewis acid catalyzed synthesis and host–guest property, J. Am. Chem. Soc. 130 (2008) 5022–5023.
[8] T. Ogoshi, T.A. Yamagishi, Pillararenes: versatile synthetic receptors for supramolecular chemistry, Eur. J. Org. Chem. 2013 (2013) 2961–2975.
[9] X. Tan, Y. Liu, T. Zhang, S. Luo, X. Liu, H. Tian, Y. Yang, C. Chen, Ultrasensitive electrochemical detection of methyl parathion pesticide based on cationic water-soluble pillar [5]arene and reduced graphene nanocomposite, RSC Adv. 9 (2019) 345–353.
[10] Y. Sun, F. Zhang, J. Quan, F. Zhu, W. Hong, J. Ma, H. Pang, Y. Sun, D. Tian, H. Li, A biomimetic chiral-driven ionic gate constructed by pillar [6]arene-based host–guest systems, Nat. Commun. 9 (2018) 2617.
[11] J.L. Zhang, X.W. Zhang, B. Yuan, H. Zhang, X.Z. Wang, H. Wang, H.W. Zhao, Supramolecular chemotherapy: complexation by carboxylated pillar [6]arene for decreasing cytotoxicity of nitrogen mustard to normal cells and enhancing its antitumor efficiency against breast cancer, ACS Omega 9 (2024) 11829–11835.
[12] Y. Zhang, M. Ma, L. Chen, X. Du, Z. Meng, H. Zhang, Z. Zheng, J. Chen, Q. Meng, A biocompatible liquid pillar[n]arene-based drug reservoir for topical drug delivery, Pharmaceutics (2022) 2621.
[13] X. Ran, Q. Qu, X. Qian, W. Xie, S. Li, L. Li, L. Yang, Water-soluble pillar [6]arene functionalized nitrogen-doped carbon quantum dots with excellent supramolecular

recognition capability and superior electrochemical sensing performance towards TNT, Sens. Actuators B Chem. 257 (2018) 362–371.
[14] R.V. Shamagsumova, D.N. Shurpik, Y.I. Kuzin, I.I. Stoikov, A.M. Rogov, G. A. Evtugyn, Pillar [6]arene: electrochemistry and application in electrochemical (bio)sensors, J. Electroanal. Chem. 913 (2022) 116281.
[15] X. Feng, J. Wu, P. Liao, J. Guo, Z. Li, R. Lin, Z. Chi, J. Zhang, S.L. James, Pillararene for fluorescence detection of n-alkane vapours, Mater. Chem. Front. 5 (2021) 7910–7920.
[16] Q. Zhang, J. Li, T.-J. Yue, N. Li, Y.-Q. Jiang, H.-M. Guo, Linking electron-rich Pillar [5]arene into hyper-cross-linked polymers for highly effective adsorption of iodine vapor, J. Solid. State Chem. 331 (2024) 124528.
[17] E. Li, K. Jie, Y. Fang, P. Cai, F. Huang, Transformation of nonporous adaptive pillar [4]arene [1]quinone crystals into fluorescent crystals *via* multi-step solid–vapor postsynthetic modification for fluorescence turn-on sensing of ethylenediamine, J. Am. Chem. Soc. 142 (2020) 15560–15568.
[18] Q. Lin, Y.Q. Fan, G.F. Gong, P.P. Mao, J. Wang, X.W. Guan, J. Liu, Y.-M. Zhang, H. Yao, T.-B. Wei, Ultrasensitive detection of formaldehyde in gas and solutions by a catalyst preplaced sensor based on a pillar [5]arene derivative, ACS Sustain. Chem. Eng. 6 (2018) 8775–8781.
[19] W.B. Zhu, T.B. Wei, Y.Q. Fan, W.J. Qu, W. Zhu, X.Q. Ma, H. Yao, Y.M. Zhang, Q. Lin, A pillar [5]arene-based and OH− dependent dual-channel supramolecular chemosensor for recyclable CO_2 gas detection: high sensitive and selective off-on-off response, Dyes Pigments 174 (2020) 108073.
[20] A.N. Kursunlu, Y. Acikbas, C. Yilmaz, M. Ozmen, I. Capan, R. Capan, K. Buyukkabasakal, A. Senocak, Sensing volatile pollutants with spin-coated films made of pillar [5]arene derivatives and data validation *via* artificial neural networks, ACS Appl. Mater. Interfaces. 16 (2024) 31851–31863.
[21] R. Liu, M. Li, Z. Liu, B. Hua, Separation of cyclohexanol from cyclohexanol/cyclohexene mixtures by crystals of pillar [6]arene containing three benzoquinone units, Chem. Commun. 60 (2024) 7626–7629.
[22] H. Roithmeyer, J. Bühler, O. Blacque, I. Tuncay, T. Moehl, C. Invernizzi, F. Keller, M. Iannuzzi, D. Tilley, The Swiss army knife of electrodes: pillar [6]arene-modified electrodes for molecular electrocatalysis over a wide pH range, Angew. Chem. Int. Ed. n/a (2024) e202413144.
[23] B. Shi, W. Li, P. Qin, T.B. Wei, W.J. Qu, Y. Liu, Q. Lin, Capture and removal of iodine by a fluorinated leaning pillar [6]arene with host–guest interactions, ChemNanoMat 9 (2023) e202300156.
[24] S. Ohtani, K. Nakaguchi, K. Kato, T. Ogoshi, Solid-state emissive pillar [6]arene derivative having alternate methylene and nitrogen bridges, Chem. Asian J. 19 (2024) e202400106.
[25] K. Wada, S. Ohtani, K. Kato, T. Ogoshi, Stable planar chirality of arylated pillar [6]arene and its thermal response, Tetrahedron. Lett. 135 (2024) 154891.
[26] Y. Acikbas, M. Aksoy, M. Aksoy, D. Karaagac, E. Bastug, A.N. Kursunlu, M. Erdogan, R. Capan, M. Ozmen, M. Ersoz, Recent progress in pillar[n]arene-based thin films on chemical sensor applications, J. Incl. Phenom. Macrocycl. Chem. 100 (2021) 39–54.
[27] Y. Acikbas, A.N. Kursunlu, M. Ozmen, R. Capan, M. Erdogan, G. Kucukyildiz, An aminopyridine bearing pillar [5]arene-based QCM sensor for chemical sensing applications: design, experimental characterization, data modeling, and prediction, IEEE Sens. J. 20 (2020) 14732–14739.
[28] A.N. Kursunlu, Y. Acikbas, M. Ozmen, M. Erdogan, R. Capan, Haloalkanes and aromatic hydrocarbons sensing using Langmuir–Blodgett thin film of pillar [5]arene-biphenylcarboxylic acid, Colloids Surf. Physicochem. Eng. Asp. 565 (2019) 108–117.
[29] A.N. Kursunlu, Y. Acikbas, M. Ozmen, M. Erdogan, R. Capan, Fabrication of LB thin film of pillar [5]arene-2-amino-3-hydroxypyridine for the sensing of vapors, Mater. Lett. 267 (2020) 127538.
[30] M. Ozmen, A.N. Kursunlu, Y. Acikbas, M. Erdogan, R. Capan, Investigation of environmentally volatile pollutants sensing using pillar [5]arene-based macrocycle Langmuir–Blodgett film, Appl. Phys. A 126 (2020) 212.
[31] Y. Acikbas, A.N. Kursunlu, M. Ozmen, K. Buyukkabasakal, M. Erdogan, R. Capan, Stability evaluation of environmentally volatile pollutants sensing devices by developing theoretical calculation and mathematical modeling, Sens. Actuators Phys. 333 (2022) 113216.
[32] K. Atacan, A.N. Kursunlu, M. Ozmen, Preparation of pillar [5]arene immobilized trypsin and its application in microwave-assisted digestion of cytochrome *c*, Mater. Sci. Eng. C 94 (2019) 886–893.
[33] S. Santra, I.S. Kovalev, D.S. Kopchuk, G.V. Zyryanov, A. Majee, V.N. Charushin, O. N. Chupakhin, Role of polar solvents for the synthesis of pillar [6]arenes, RSC. Adv. 5 (2015) 104284–104288.
[34] W. Knoll, Interfaces and thin films as seen by bound electromagnetic waves, Annu. Rev. Phys. Chem. 49 (1998) 569–638.
[35] M. Rodin, D. Helle, D. Kuckling, Pillar [5]arene-based dually crosslinked supramolecular gel as a sensor for the detection of adiponitrile, Polym. Chem. 15 (2024) 661–679.
[36] S. Ekgasit, A. Tangcharoenbumrungsuk, F. Yu, A. Baba, W. Knoll, Resonance shifts in SPR curves of nonabsorbing, weakly absorbing, and strongly absorbing dielectrics, Sens. Actuators. B Chem. 105 (2005) 532–541.
[37] X. Fan, B. Du, Selective detection of trace p-xylene by polymer-coated QCM sensors, Sens. Actuators. B Chem. 166-167 (2012) 753–760.
[38] K. Triyana, A. Rianjanu, D.B. Nugroho, A.H. As'ari, A. Kusumaatmaja, R. Roto, R. Suryana, H.S. Wasisto, A highly sensitive safrole sensor based on polyvinyl acetate (PVAc) nanofiber-coated QCM, Sci. Rep. 9 (2019) 15407.
[39] A. Rianjanu, K. Triyana, D.B. Nugroho, A. Kusumaatmaja, R. Roto, Electrospun polyvinyl acetate nanofiber modified quartz crystal microbalance for detection of primary alcohol vapor, Sens. Actuators A Phys. 301 (2020) 111742.
[40] Y. Acikbas, G. Dogan, M. Erdoğan, R. Çapan, C. Soykan, Organic vapor sensing properties of copolymer Langmuir-Blodgett thin film sensors, J. Macromol. Sci. A 53 (2016) 470–474.
[41] K. Büyükkabasakal, S.C. Acikbas, A. Deniz, Y. Acikbas, R. Capan, M. Erdogan, Chemical sensor properties and mathematical modeling of graphene oxide Langmuir-Blodgett thin films, IEEE Sens. J. 19 (2019) 9097–9104.